

Corrosion of Structural Alloys in High-Temperature
Molten Fluoride Salts for Applications in Molten Salt
Reactors

Download PDF




Download PDF



- Nuclear Materials, Oxidation, Supercritical CO₂, and Corrosion Behavior
- [Published: 26 June 2018](#)

Corrosion of Structural Alloys in High-Temperature Molten Fluoride Salts for Applications in Molten Salt Reactors

- [Guiqiu Zheng](#) &
- [Kumar Sridharan](#) 

[JOM](#) **70**, 1535–1541 (2018)

- 5534 Accesses
- 1 Altmetric
- [Metrics](#)

Abstract

Hastelloy N[®], a nickel-based alloy, and 316 stainless steel are among the candidate structural materials being considered for the construction of the molten salt reactor (MSR). Most of the proposed MSR concepts use molten fluoride salts as coolant which can be quite corrosive to structural alloys. The

results of studies on the corrosion behavior of the two alloys in molten Li_2BeF_4 (FLiBe) salt at 700°C are discussed. This salt is being considered as the primary coolant for MSR designs featuring solid fuel particles, but the reported results also provide insights into the corrosion in MSR designs where the uranium fuel is dissolved in the molten fluoride salt. Corrosion was observed to occur predominantly by de-alloying of Cr from the alloy surface and into the molten salt, with more pronounced attack occurring along the grain boundaries than in the bulk grains. The magnitude and the mechanisms of corrosion were different for corrosion tests performed in graphite and metallic capsules, a result warranting recognition given the coexistence of structural alloys and graphite in the molten salt medium in the MSR.

Introduction

Currently, molten salt reactors (MSR) feature two designs. One is the molten salt-fueled reactor in which the fuel salt is dissolved in the coolant salt. An example of this design is the well-known Molten Salt Reactor Experiment (MSRE) that was successfully implemented at the Oak Ridge National Laboratory (ORNL) in the U.S. during 1960–70s.[1,2,3](#) The second design uses the molten salt as a coolant in conjunction with solid, SiC coated tristructural isotropic (TRISO) fuel particles immersed in the salt coolant. The SiC coating is provided for fission product containment. This second design is referred to as the fluoride salt-cooled high-temperature reactor (FHR), and ^7Li -enriched Li_2BeF_4 (FLiBe) salt is emerging as the lead primary coolant for the FHR.[4,5,6](#)

The MSR is presently attracting considerable interest because it provides for a number of key benefits, including: (1) a high degree of passive safety, (2) atmospheric pressure operation, (3) high thermal efficiency due to high volumetric heat capacity and thermal conductivity of molten salts, (4) lower spent fuel per unit energy, and (5) high solubility of most fission products in molten salts.[4,5](#) The fluoride salts being considered for the MSR have high boiling points ($> 1000^\circ\text{C}$) making a loss of coolant accident scenario highly unlikely, while also allowing for higher operation temperatures with the associated higher thermodynamic efficiencies. Thus, the

MSRs are anticipated to meet the aim of developing a set of safe, sustainable, efficient, and low cost commercial nuclear reactors in the Generation IV International Forum.[7](#)

The corrosion of structural alloys in molten fluoride salts is recognized as an important consideration in the successful fruition of MSRs. The protective surface oxide layer that is relied upon for corrosion protection in most high-temperature environments is generally unstable in molten fluoride salts.[8](#) Alloying elements promoting the formation of protective oxide layers such as Cr, Al, and Si are prone to dissolution in molten fluoride salts. Such corrosion can lead to the thinning of structural components, and, additionally, the corrosion products can plate-out on the relatively cooler sections of the reactor system due to the strong dependence of solubility on temperature. The corrosion can be driven by impurities in the salt and thermal gradients in the reactor system, as well as the presence of dissimilar materials in the molten salt.[9](#) In the reactor environment, the strong radiation fields can exacerbate alloy corrosion in molten salt, but the mechanisms are not conclusively understood.[10](#)

Hastelloy N[®] and 316 stainless steel are being actively considered as structural materials for the FHR, and corrosion experiments of these alloys in either static or dynamic systems have been conducted in laboratories to support the development of the FHR.[11,12,13,14,15](#) This work provides a brief overview of the corrosion results of these two alloys in molten FLiBe salt, and the role of graphite on corrosion.

Experimental Method

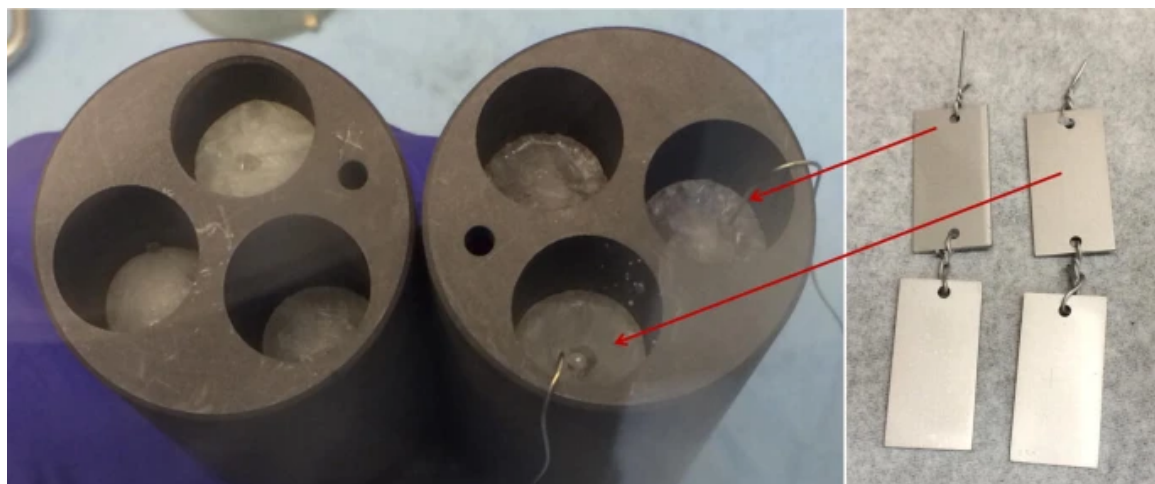
The alloys discussed in this study are commercial purity 316L stainless steel and Hastelloy N[®]. Hastelloy N[®], a low-Cr, high-Mo Ni-based alloy, was developed during the MSRE program specifically for use in molten fluoride salt environments. 316L stainless steel is ASME code certified to operate at 700°C, the intended operating temperature of FHR. The nominal compositions of the sheets of the two alloys used in this study are listed in Table [I](#).

Table I Nominal compositions of Hastelloy N[®] and 316L stainless steel (in wt.%) used in this study

The as-received sheets of the alloy were sectioned to dimensions of $\sim 13 \text{ mm} \times 7 \text{ mm} \times 1 \text{ mm}$ and mechanically ground to 1200-grit final finish, and cleaned in deionized water and acetone prior to introduction into the molten salt. The fluoride molten salt used in this study was FLiBe, provided by ORNL and originally from the MSRE program. The salt was re-melted and purified by a hydrofluorination process followed by additions of small amounts of beryllium to achieve a stable low redox potential of the salt.

Figure 1 shows the graphite capsules and samples for high-temperature static corrosion tests in FLiBe salt. The capsules were prepared by machining cylindrical compartments in a cylindrical nuclear-grade graphite block so that multiple materials could be tested simultaneously under identical conditions. This design also allowed for 316 stainless steel and pure nickel liners to be inserted into the capsules to prevent the molten salt from contacting the graphite, in effect creating a metallic containment (or capsules) for corrosion testing within the graphite capsules. The containment material influences the mechanism and extent of corrosion of the test samples in molten salt environments.¹⁶ The polished alloy samples were suspended using 316 stainless steel wire for the 316 stainless steel samples, and pure nickel wire (99.98% Alfa Aesar) for the Hastelloy N[®] samples, then loaded into crucibles, followed by filling with purified and Be-reduced FLiBe salt in a liquid state. The graphite capsules and lined capsules were filled with approximately 18 g and 10 g FLiBe salt, respectively. All handling of the salt and corrosion testing was performed in an argon-backfilled glove box to prevent salt contamination and for personnel safety. Corrosion testing was performed in a cylindrical ceramic furnace inside the glove box, at 700°C.

Fig. 1



Graphite capsules (left) for high-temperature static corrosion tests in molten FLiBe salt, and samples of 316 stainless steel samples (right) taken out of the molten salt after the 1000-h corrosion test

After corrosion, the tested samples were removed from the molten salt by pulling out the hanging wires, then cooled in the glove box. The samples were cleaned and sectioned for further microstructural characterization. The samples evaluated in this study and the test conditions are summarized in Table II. The microstructure of the surfaces and cross-sections of the samples were characterized by using a scanning electron microscope (SEM) equipped with energy dispersive spectroscopy (EDS).

Table II Summary of samples and test conditions used in this study

Results and Discussion

Corrosion of Hastelloy N[®] in Molten FLiBe Salt

Hastelloy N[®] (Alloy N, UNS10003) is the trade name of the nickel-based alloy that was originally developed during the MSRE program at the ORNL (initially named INOR-8) specifically for combining the resistance to corrosion in molten fluoride salts and air-side oxidation.^{17,18,19,20,21} The high concentrations of nickel and molybdenum in this alloy enhance its corrosion resistance in molten fluoride salt and its high-temperature strength. The highly successful performance of this alloy and the accumulated experience in the MSRE program makes it a lead candidate for consideration as a structural alloy in FHR and other future MSR concepts.²¹ However, the alloy is not code certified in

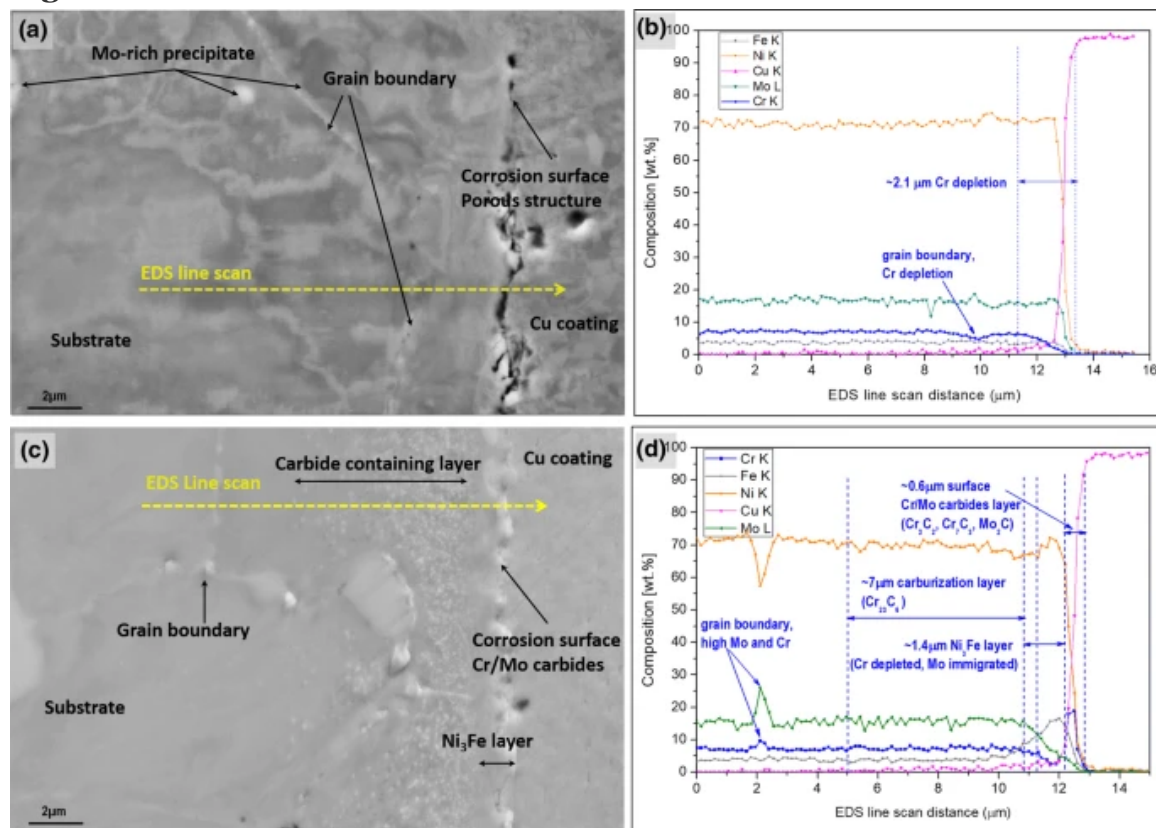
the ASME Boiler Pressure Vessel Code under sections I, III, B31.1 and B31.3 for the applications in commercial reactors.²² Therefore, further testing and evaluation of this alloy is needed at temperatures in excess of those used in the MSRE program.

The high-temperature static corrosion tests of Hastelloy N[®] in molten FLiBe salt at 700°C for 1000 h have been recently accomplished in nickel and graphite capsules. The results suggest that the Hastelloy N[®] samples tested in nickel capsules experience very little attack in terms of the alloy's near-surface Cr depletion into the salt. The dissolution of the alloying elements, primarily Cr, results in the formation of a thin porous layer in the near-surface regions of the alloy. The corrosion-induced porous structure results from the coalescence of voids that form due to Cr leaching into the salt from the alloy matrix at high temperature.²³ However, when tested in the graphite capsules, a large number of carbide particulate phases formed in the near-surface regions [mainly Cr₃C₂, Cr₇C₃, Mo₂C, and (Cr, Mn)₂₃C₆ particles] extending to approximately 7 μm in addition to the Cr depletion preferentially along grain boundaries.¹⁴

The cross-sectional SEM–EDS results quantifying the nature and depth of corrosion attack in the Hastelloy N[®] tested in the pure nickel and graphite capsules are shown in Fig. 2. Figure 2a and b present the cross-section and the concentration profiles of the principal elements along the EDS line scan for the sample tested in the pure nickel capsules. Mo- and Si-rich precipitates were observed both at and in the vicinity of the grain boundaries. The Cr concentration profile indicates a Cr-depletion depth of approximately 2.1 μm. For the sample tested in the graphite capsules, multiple corrosion-affected layers with varying structures and compositions were observed and are separated by vertical dashed lines in Fig. 2d corresponding to the microstructural observations in Fig. 2c. The Cr profile shows approximately 0.6 μm of a high chromium-carbide rich zone. Underneath this, an approximately 1.4-μm-deep zone of a Ni₃Fe alloy layer develops due to the compositional shifts caused by the corrosion process. In a grain boundary approximately 10 μm beneath the surface, the relatively high

concentration of Mo and Cr indicates the thermal diffusion of these two elements preferentially toward the grain boundaries within the alloy. In the carbide-containing layer of approximately $7\ \mu\text{m}$ in depth, the Cr concentration is slightly higher than in the matrix. This carbide-containing layer results from the reactions between Cr in the Hastelloy N[®] matrix and the inward diffusing carbon from the molten salt. The carbon source in the molten salt originally emanated from the graphite surface. The Cr in the near-surface region diffused outward to react with carbon on the alloy's surface to form chromium carbides in the initial stage of corrosion. Meanwhile, the carbon in the FLiBe salt diffused inward and reacted with the Cr in the deeper alloy matrix because the diffusion rate of carbon through the nickel ($D_{\text{C/Ni}} \sim 10^{-6}\ \text{cm}^2/\text{s}$) is much faster than through Cr ($D_{\text{Cr/Ni}} \sim 10^{-11}\ \text{cm}^2/\text{s}$) at 700°C .^{24,25}

Fig. 2



Adapted from Ref. [14](#).

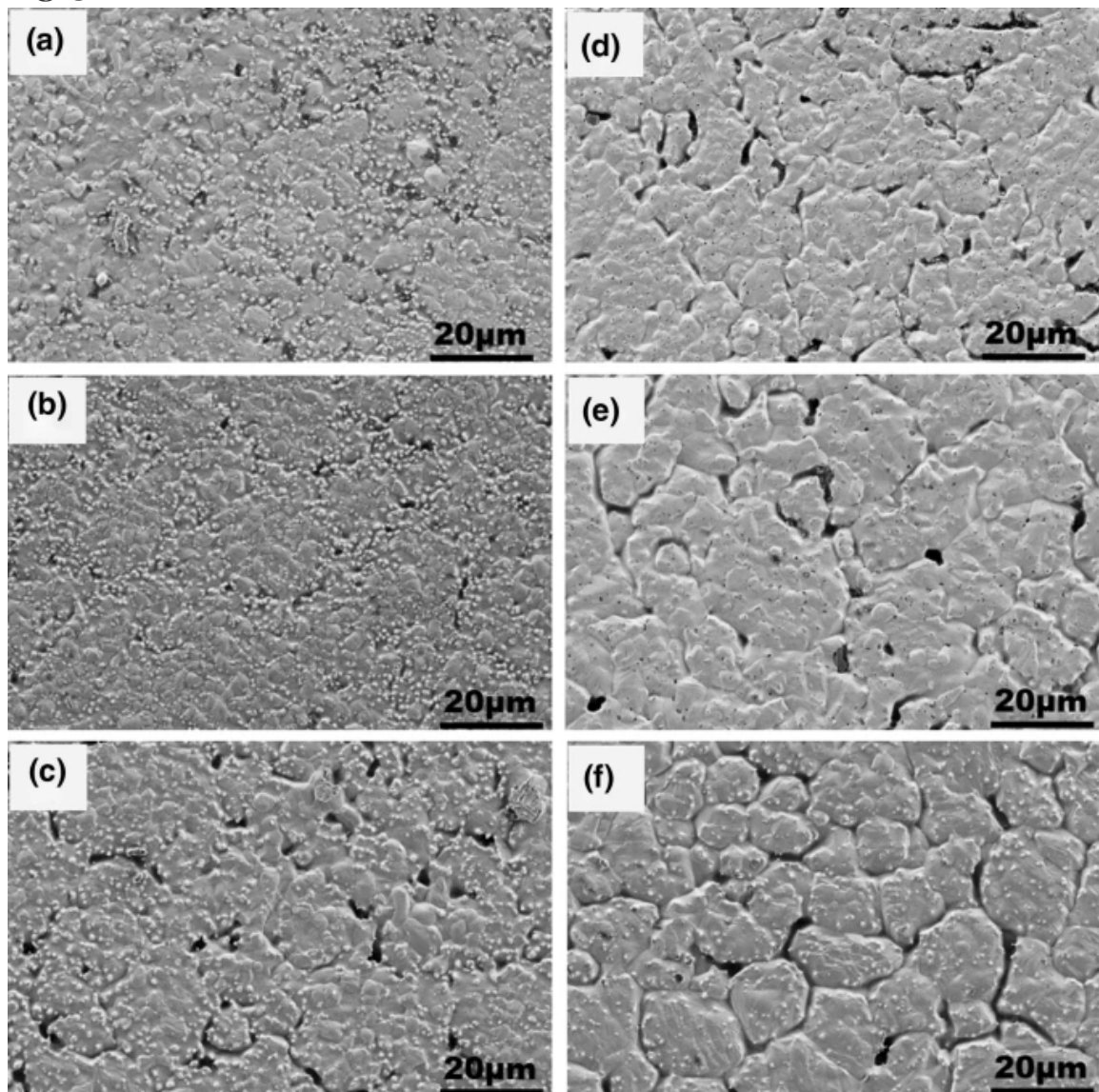
SEM–EDS analysis of Hastelloy N[®] samples tested in the (a, b) nickel capsules and (c, d) graphite capsules. Electroplated Cu coating was applied on the surface of the samples for edge retention during polishing. Yellow dashed arrows in the

cross-sectional SEM images denote the traces of the EDS line scan.

Corrosion of 316 Stainless Steel in Molten FLiBe Salt

316 stainless steel has been widely used in high-temperature environments due to its excellent mechanical properties and phase stability at high temperature. It is being strongly considered as the first-wall and blanket material for the first generation TOKAMAK-type fusion reactors in which FLiBe salt will be used as coolant-breeding material.²⁶ A thermal convection loop was constructed with 316 stainless steel under the MSRE program to investigate its compatibility with molten FLiBe salt.²⁶ The corrosion rate was calculated to be about 10 $\mu\text{m}/\text{year}$ and even less when Be metal was added as reducing agent into the molten salt. However, the corrosion mechanisms at a microstructural level were not fully investigated in these earlier studies. Recently, 316 stainless steel is being actively considered as the structural material for the FHR and other MSR concepts because of its existing code certification at the intended FHR operation temperatures. The corrosion performance of this alloy in molten FLiBe salt must be investigated to provide data for its potential applications in the FHR in the future, both without and in the presence of graphite. We report here the results of static corrosion tests of 316 stainless steel conducted in 316 stainless steel and in graphite capsules.

The surface images of 316 stainless steel samples after the corrosion tests in 316 stainless steel and graphite capsules for 1000 h, 2000 h, and 3000 h are shown in Fig. 3. Corrosion attack is clearly evident in the near-surface regions particularly along the grain boundaries, in addition to the attack in the grains. The degree of attack increases with exposure time. No surface oxide layers are observed. The samples tested in the graphite capsules had relatively deeper grain boundary attack than those tested in the 316 stainless steel capsules. These initial observations indicate that graphite accelerates the corrosion attack to 316 stainless steel. Additionally, pitting was observed on the grains of all the samples, and there was evidence of MoSi_2 particulates adhered to the surface.²⁷

Fig. 3

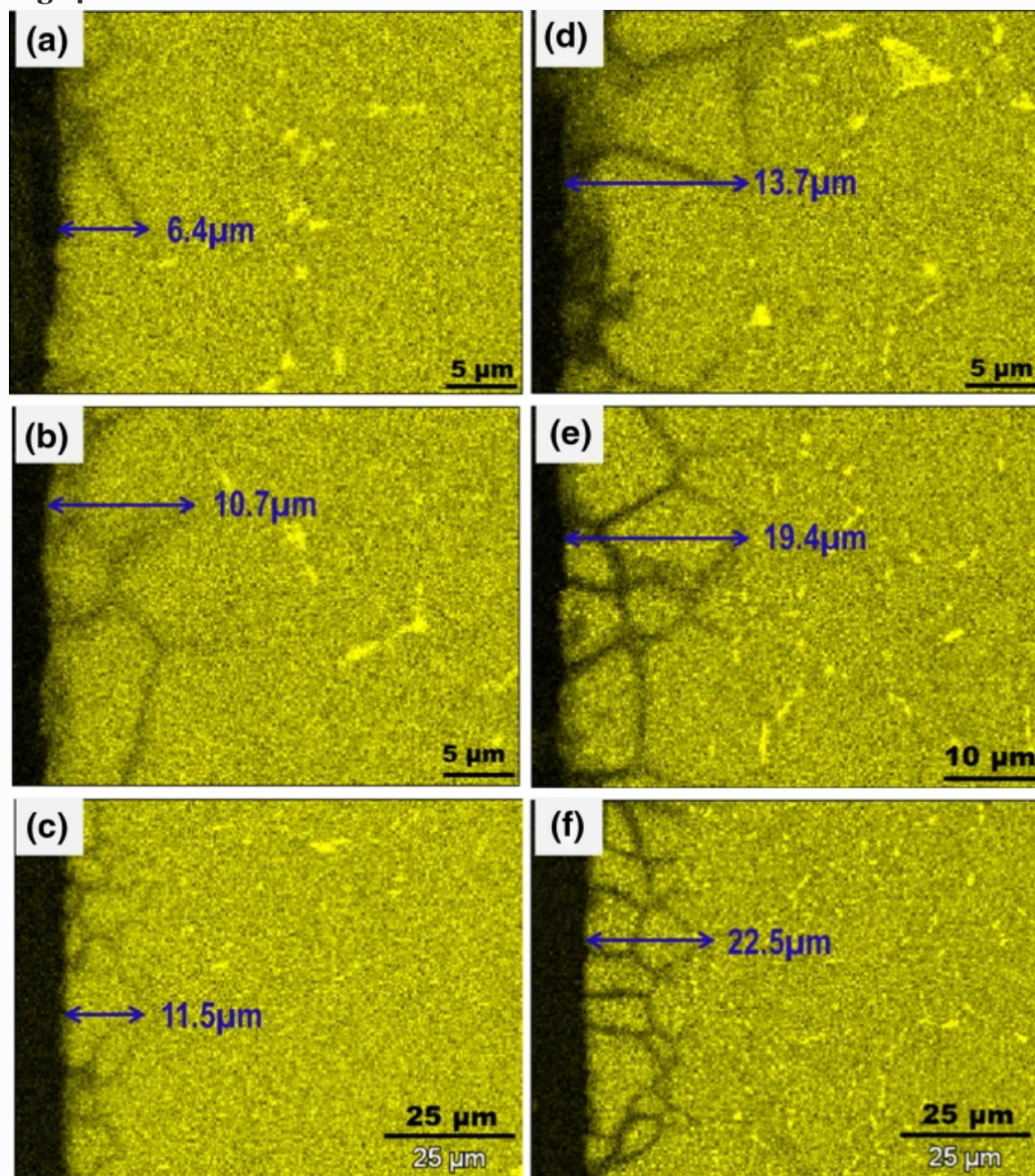
Reprinted with the permission from Ref. [13](#)

SEM surface images of 316 stainless steel samples after corrosion testing: (a–c) tested in 316 stainless steel capsules and (d–f) tested in graphite capsules at 700°C for 1000 h, 2000 h, and 3000 h, respectively.

The depth of corrosion attack was measured in terms of the maximum Cr depletion distance using EDS elemental maps for Cr as shown in Fig. [4](#). The corrosion attack depth was found to be from 6.4 μm to 11.5 μm for the samples tested in 316 stainless steel capsules, and from 13.7 μm to 22.5 μm for the samples tested in graphite capsules for corrosion exposure times from 1000 h to 3000 h. Increasing the corrosion time increased the affected depth, and testing in graphite capsules increased the maximum Cr depletion depth. Based on the experimental data, the long-term corrosion attack depth may be approximately predicted from curve-

fitting as shown in Fig. 5. The fits predict an attack depth of $17.1\ \mu\text{m}/\text{year}$ and $31.2\ \mu\text{m}/\text{year}$ for the samples tested in 316 stainless steel capsules and graphite capsules, respectively. In addition to the preferential Cr depletion along the grain boundaries, the EDS maps also showed Cr depletion from the bulk grains in a shallow region near the corrosion surface. This can be seen in Fig. 4d where grain depletion of Cr accounts for a layer approximately $3\ \mu\text{m}$ thick.

Fig. 4

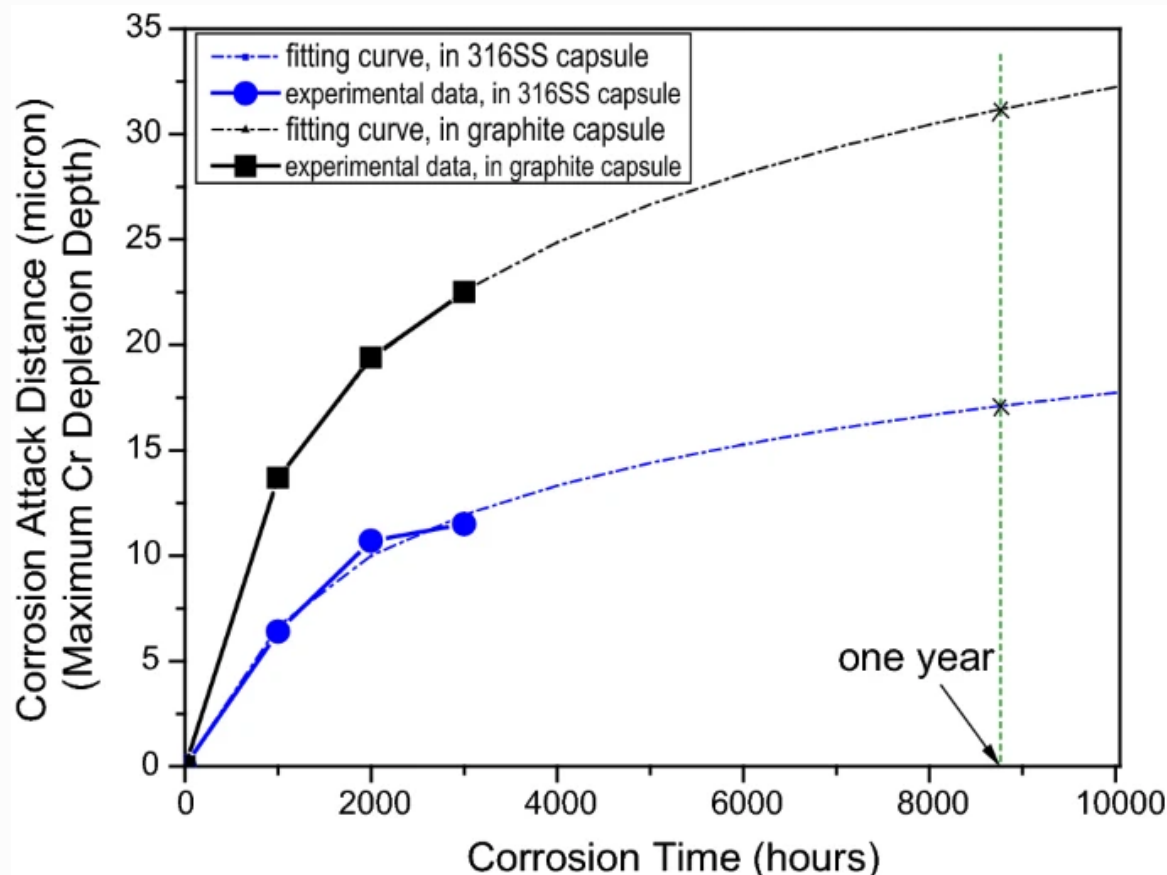


Reprinted with permission from Ref. 13 (Color figure online)

EDS maps of Cr as a function of depth below the surface of 316 stainless steel samples after corrosion tests: (a–c) tested in 316 stainless steel capsule and (d–f) tested in graphite

capsule for 1000 h, 2000 h, and 3000 h, respectively. The maximum Cr depletion distance along grain boundaries is labeled in each EDS Cr map.

Fig. 5



Reprinted with permission from Ref. 13

The experimental data of corrosion attack depth as a function of corrosion time, and extrapolation of data to longer exposure times.

Conclusion

The recent static corrosion results of Hastelloy N[®] and 316 stainless steel in molten FLiBe salt at 700°C have been reviewed. Corrosion in molten FLiBe (and other fluoride salts) occurs by de-alloying of Cr from the alloy into the molten salt with a more accelerated attack along the grain boundaries than in the grains. For Hastelloy N[®] tested in Ni capsules, a thin porous structured layer developed in the near-surface regions of the corrosion surface, and a large number of Mo-rich precipitates were observed to form at the grain boundaries. For tests carried out in graphite capsules, carbide phases (Cr₃C₂, Cr₇C₃, Mo₂C) formed in the near-

surface regions of the alloy, in addition to Cr depletion and concurrent formation of a Ni_3Fe phase layer approximately $1.4\text{ }\mu\text{m}$ deep in the near-surface region. 316 stainless steel tests performed in graphite capsules exhibited about twice the attack depth compared to the samples tested in 316 stainless steel capsules. In both cases, the trends in the depth of corrosion attack are indicative of a self-limiting kinetics. Overall, Hastelloy N[®] showed better corrosion resistance than 316 stainless steel to the molten FLiBe salt at 700°C .

References

1. 1.
R.C. Robertson, Report No. ORNL-TM-728, Oak Ridge National Laboratory, Oak Ridge, TN, January 1965.
2. 2.
R.E. Thoma, Report No. ORNL-4658, Oak Ridge National Laboratory, Oak Ridge, TN, December 1971.
3. 3.
H.G. Macpherson, *Nucl. Sci. Eng.* 90, 374 (1985).
4. 4.
D.E. Holcomb, G.F. Flanagan, G.T. Mays, W.D. Pointer, K.R. Robb, and G.L. Yoder, Report No. ONRL/TM-2013/401, Oak Ridge National Laboratory, Oak Ridge, TN, September 2013.
5. 5.
G.F. Flanagan, D.E. Holcomb, and S.M. Cetiner, Report No. ORNL/TM-2012/226, Oak Ridge National Laboratory, Oak Ridge, TN, June 2012.
6. 6.
C.W. Forsberg, L.W. Hu, P.F. Peterson, M. Fratoni, K. Sridharan, and E. Blandford, *Trans. Am. Nucl. Soc.* 116, 21808 (2017).
7. 7.
J. Serp, M. Allibert, O. Benes, S. Delpech, O. Feynberg, V. Ghetta, D. Heuer, D. Holcomb, V. Ignatiev, J.

Kloosterman, L. Luzzi, E. Merle-Lucotte, J. Uhlir, R. Yoshioka, and Z. Dai, *Prog. Nucl. Energy* 77, 308 (2014).

8. 8.

L.C. Olson, J.W. Ambrosek, K. Sridharan, M.H. Anderson, and T.R. Allen, *J. Fluor. Chem.* 130, 67 (2009).

9. 9.

K. Sridharan and T.R. Allen, *Molten Salts Chemistry, From Lab to Applications, Ch. 12*, ed. F. Lantelme and H. Groult (Amsterdam: Elsevier, 2013), p. 241.

10. 10.

G. Zheng, D. Carpenter, L. Hu, and K. Sridharan, *Adv. Mater. Sci. Environ. Energy Technol. V Ceram. Trans.* 260, 93 (2016).

11. 11.

L.C. Olson, Materials corrosion in molten LiF-NaF-KF eutectic salt, Ph.D. dissertation, University of Wisconsin-Madison, 2009,
<http://allen.neep.wisc.edu/docs/dissertation-olson-luke.pdf>. Accessed 21 Oct 2011.

12. 12.

G. Zheng, Corrosion behavior of alloys in molten fluoride salts, Ph.D. dissertation, University of Wisconsin-Madison, 2015,
https://www.academia.edu/22949975/Corrosion_Behavior_of_Alloys_in_Molten_Fluoride_Salts. Accessed 29 July 2015.

13. 13.

G. Zheng, B. Kelleher, G. Cao, M. Anderson, T. Allen, and K. Sridharan, *J. Nucl. Mater.* 461, 143 (2015).

14. 14.

G. Zheng, B. Kelleher, L. He, G. Cao, M. Anderson, T. Allen, and K. Sridharan, *CORROSION* 71, 1257 (2015).

15. 15.

G.L. Yoder Jr, A. Aaron, B. Cunningham, D. Fugate, D. Holcomb, R. Kisner, F. Peretz, K. Robb, J. Wilgen, and D. Wilson, *Ann. Nucl. Energy* 64, 511 (2014).

16. 16.

L.C. Olson, R.E. Fuentes, M.J. Martinez-Rodriguez, J.W. Ambrosek, K. Sridharan, M.H. Anderson, B.L. Garcia-Diaz, J. Gray, and T.R. Allen, *J. Sol. Energy Eng.* 137, 61007 (2015).

17. 17.

H.E. McCoy and B. McNabb, Report No. ORNL-4829, Oak Ridge National Laboratory, Oak Ridge, TN, November 1972.

18. 18.

J.W. Koger, Report No. ORNL-TM-4189, Oak Ridge National Laboratory, Oak Ridge, TN, December 1972.

19. 19.

J.H. DeVan and R.B. Evans, Report No. ORNL-TM-328, Oak Ridge National Laboratory, Oak Ridge, TN, September 1962.

20. 20.

R.E. Gehlbach and H.E. McCoy, in *International Symposium on Structural Stability in Superalloys* (1968), p. 346,
http://www.tms.org/superalloys/10.7449/1968/Superalloys_1968_346_366.pdf.
Accessed 14 Oct 2013.

21. 21.

W.J. Ren, D.F. Wilson, G. Muralidharan, and D.E. Holcomb, in *Proceedings of the ASME 2011 Pressure Vessels and Piping Division Conference* (2011).

22. 22.

H.J. White, Haynes International Capabilities: HASTELLOY N alloy, Presentation at Oak Ridge National Laboratory, Oak Ridge, TN, September 2010.

23. 23.

L.S. Richardson, D.E. Vreeland, and W.D. Manly, Report No. ORNL-1491, Oak Ridge National Laboratory, Oak Ridge, TN, March 1953.

24. 24.

S.P. Murarka, M.S. Anand, and R.P. Agarwala, *J. Appl. Phys.* 35, 1339 (1964).

25. 25.

B.S. Berry, *J. Appl. Phys.* 44, 3792 (1973).

26. 26.

J.R. Keiser, J.H. DeVan, and D.L. Manning, Report No. ORNL/TM-5782, Oak Ridge National Laboratory, Oak Ridge, TN, April 1977.

27. 27.

G. Zheng, L. He, D. Carpenter, and K. Sridharan, *J. Nucl. Mater.* 482, 147 (2016).

Acknowledgements

This work was supported by the U.S. Department of Energy Integrated Research Project Nuclear Energy University Program under Contract No. DE-NE0008285.

Author information

Affiliations

1. Nuclear Reactor Laboratory, Massachusetts Institute of Technology, Cambridge, MA, 02139, USA

Guiqiu Zheng

2. Department of Engineering Physics, University of Wisconsin-Madison, Madison, WI, 53706, USA

Guiqiu Zheng & Kumar Sridharan

3. Department of Materials Science and Engineering, University of Wisconsin-Madison, Madison, WI, 53706, USA

Guiqiu Zheng & Kumar Sridharan

Corresponding author

Correspondence to Kumar Sridharan.

Rights and permissions

[Reprints and Permissions](#)

About this article

Cite this article

Zheng, G., Sridharan, K. Corrosion of Structural Alloys in High-Temperature Molten Fluoride Salts for Applications in Molten Salt Reactors. *JOM* **70**, 1535–1541 (2018).
<https://doi.org/10.1007/s11837-018-2981-2>

- Received 18 April 2018
- Accepted 11 June 2018
- Published 26 June 2018
- Issue Date August 2018
- DOI <https://doi.org/10.1007/s11837-018-2981-2>

Share this article

Anyone you share the following link with will be able to read this content:

Get shareable link

Provided by the Springer Nature SharedIt content-sharing initiative

Not logged in - 124.187.110.32

Not affiliated

SPRINGER NATURE

© 2021 Springer Nature Switzerland AG. Part of [Springer Nature](#).

